Spray Characterization and Structure Analysis in a Model LPP Atomizer

Shirin Patil and Srikrishna Sahu

1 Introduction

The injection of liquid jet into crossflow is widely studied in literature due to its enormous industrial applications. It is employed in Lean Premixed Pre-vaporized (LPP) combustor for gas turbines which has gained popularity for its capability for NO_x reduction. This is achieved by combustion of homogeneous mixture of fuel and air at equivalence ratios close to the lean blowout limit that ensures localized regions of high temperature are always avoided in the combustor. Several studies are available in the literature which report spray characterization using different optical techniques [1–7]. Pei-Kuan et al. [6] employed Phase Doppler Particle Analyzer (PDPA) technique to measure droplet size, axial velocity, and volume flux in a spray plume. The droplet velocity was found to be uniform throughout the spray region. The sauter mean diameter (SMD) was found to increase with increase in transverse distance from the orifice and also decrease with crossflow air velocity. Becker and Hassa [1] measured spray properties for a kerosene jet injected in crossflow at elevated pressure and found weaker effect of crossflow velocity on SMD compared to that at atmospheric pressure. Tambe and Jeng [5] considered the injection of liquid jet into the swirling crossflow. The radial penetration of spray increased with increase in swirl strength and spray continued to expand further downstream due to the centrifugal forces in crossflow. However, the measurements of droplet characteristics alone are not enough for understanding on unsteadiness in sprays which is important for flame stability and optimum engine performance. Only handful studies have addressed this issue for instance, Batarseh et al. [8] reported the frequency associated with an

S. Patil (✉) · S. Sahu
Indian Institute of Technology, Madras, India
e-mail: shirin3151@gmail.com

S. Sahu
e-mail: ssahu@iitm.ac.in

airblast spray using proper orthogonal decomposition (POD) technique and found them to be equal to frequencies obtained by applying slotting technique to LDV data. The spray frequency was found to strongly depend on atomizing air velocity and atomizer geometry.

The present paper aims to experimentally study liquid jet atomization in a model twin-jet cross-stream airblast atomizer in the absence and presence of annular air swirl. The atomizer comprises of two radially opposite orifices on a central tube for liquid injection. The atomizing air flows in an annular space around the central tube. The atomizer operating conditions are selected such that any wall filming due to jet-wall interactions are avoided before the jet breakup process. The spray produced by the atomizer is visualized using laser sheet imaging and droplet measurements are taken using PDPA technique (Artium Technologies). The POD technique is applied to study spray unsteadiness and dominant structures in spray of cross-stream airblast atomizer.

2 Experimental Method

2.1 Cross-Stream Airblast Atomizer

A schematic of the twin-jet cross-stream airblast atomizer is shown in Fig. 1a. It consists of an outer cylindrical acrylic tube of 45 mm outer diameter and 39 mm inner diameter. The concentric inner cylindrical acrylic tube has 10 mm outer diameter and 6 mm inner diameter. Water enters the central tube from the top and is injected radially through opposite holes each 1 mm diameter. The holes are situated 5 mm from the end of the central tube. The end of the inner tube is kept at 10 mm above to that of the end of outer tube.
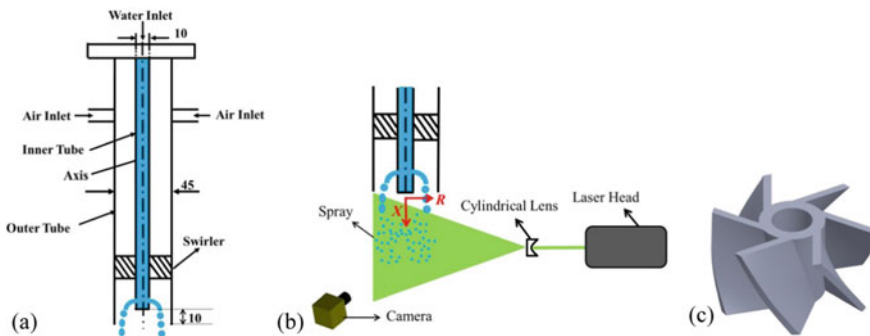

Fig. 1 a Schematic of the twin-jet cross-stream airblast atomizer. (All dimensions are in mm).
b Optical arrangement for laser sheet imaging. **c** 3D printed axial swirler

The atomizing air enters the outer tube via four radial inlets and passes through the annular gap in a direction normal to the direction of liquid exit. An in-house 3D-printed axial air swirler as shown in Fig. 1c (swirl vane angle of 45 deg, swirl number, $S = 0.74$) is placed 40 mm above the orifice to impart tangential momentum to crossflow. For the experiments in the absence of swirling air, an annular holder with straight vanes (vane angle 0°) was used. Earlier authors have done study on primary breakup characteristics of twin-jet atomizer in Patil and Sahu [9].

2.2 Optical Arrangement for Laser Sheet Imaging

A single-pulse Q smart laser (532 nm) has been used to form laser sheet using cylindrical lens as shown in Fig. 1b. Images are captured with PCO Pixelfly Camera (14 bit, 1040×1392 pixels^2) using Nikon lens (50 mm focal length; f/1.8D). The exposure time of camera was kept at 30 μs to capture the instantaneous spray image. The field of view for imaging is 150 mm × 200 mm such that the spatial resolution is 150 μm/pixel.

2.3 Injector Operating Conditions

The non-dimensional numbers for studying liquid jet breakup are defined below.

$$We_g = \frac{\rho_g U_g^2 d}{\sigma} \tag{1}$$

$$MFR = \frac{\rho_l U_l^2}{\rho_g U_g^2} \tag{2}$$

where We_g is aerodynamic Weber number, MFR is liquid-to-air momentum flux ratio, ρ_l is density of liquid water jet, U_l is liquid jet velocity, d is diameter of jet, μ_l is dynamic viscosity of water, ρ_g is density of gas, *i.e.,* air, U_g is velocity of gas, σ is surface tension for water–air interface. The flow rates of air and water in to the atomizer were varied over a wide range of We_g (40–140) and MFR (3–7) that ensure the liquid jets never hit the outer tube prior to their breakup, and the jet atomization always occurs within the annular region between the inner and outer acrylic tubes. The injector operating conditions and the corresponding non-dimensional numbers are summarized in Table 1.

Table 1 Operating conditions for cross-stream airblast atomizer

Case	U_l (m/s)	U_g (m/s)	Re_l	We_g	MFR
1	4.2	49.1	5323.8	38.9	6.4
2	4.2	68.7	5323.8	76.0	3.3
3	5.3	68.7	6654.7	76.0	5.1
4	5.3	80.1	6654.7	103.3	3.8
5	6.4	91.9	7985.7	136.2	4.1

3 Result and Discussion

3.1 Spray Characterization Using PDPA

Figure 2 shows the droplet characteristics for swirling and non-swirling crossflows at $X = 50$ mm downstream from the injector and $R = 20$ mm. It can be observed in Fig. 2a that SMD reduces with increase in We_g for swirling and non-swirling crossflows as earlier reported by Pei-Kuan et al. [6] and Takao and Nagai [4]. SMD decreases from 130 to 60 µm as We_g increases from 40 to 140 and it is observed to decrease almost linearly for swirling and non-swirling crossflows. In other words, as We_g increases by 25%, SMD decreases by 5%. It is generally expected that with the introduction of swirling crossflow, atomization quality improves and SMD reduces as compared to non-swirling crossflow but it can be clearly seen in Fig. 2a that SMD is almost similar for swirling and non-swirling crossflows at axial station of $X = 50$ mm. Droplet axial velocity (U) increases linearly with increase in We_g as can be seen in Fig. 2b. U increases from 20 to 50 m/s as We_g increases from 40 to 140. As the axial velocity of gas U_g increases, the drag force acting on the droplet increases which further increases the droplet velocity. Due to the increase in drag force on the surface of droplets, it tends to breakup, i.e., secondary atomization increases and hence SMD reduces as seen in Fig. 2a. The primary breakup regimes change from bag, multimode to surface breakup modes as We_g is increased [10–12]. Droplets are stripped off from the liquid jet surface in surface breakup mode thereby generating very small droplets and hence SMD tends to reduce as seen in Fig. 2a.

Figure 2c shows the droplet tangential velocity (V) normalized with local axial droplet velocity (U). As it is expected due to the swirling crossflow, tangential velocity is imparted to the droplets while for non-swirling crossflow, droplets have negligible tangential velocity as observed in Fig. 2c. The tangential velocity is up to 40% of axial velocity and as V/U is constant over a range of We_g, it implies that V increases with We_g. It is noted that the swirler used in the present study had swirl number ($S = 0.74$) while we measured $V/U = 0.4$. It might be because of the fact that at the end of atomizer, crossflow is allowed to expand and it is no more restricted by the outer tube and hence the swirl number is decreasing. Radial velocity of droplets (W) normalized with U (see Fig. 2d) remains constant at $W/U = 0.6$ for a range of We_g for swirling crossflow while $W/U = 0.2$ for non-swirling crossflow. It means that
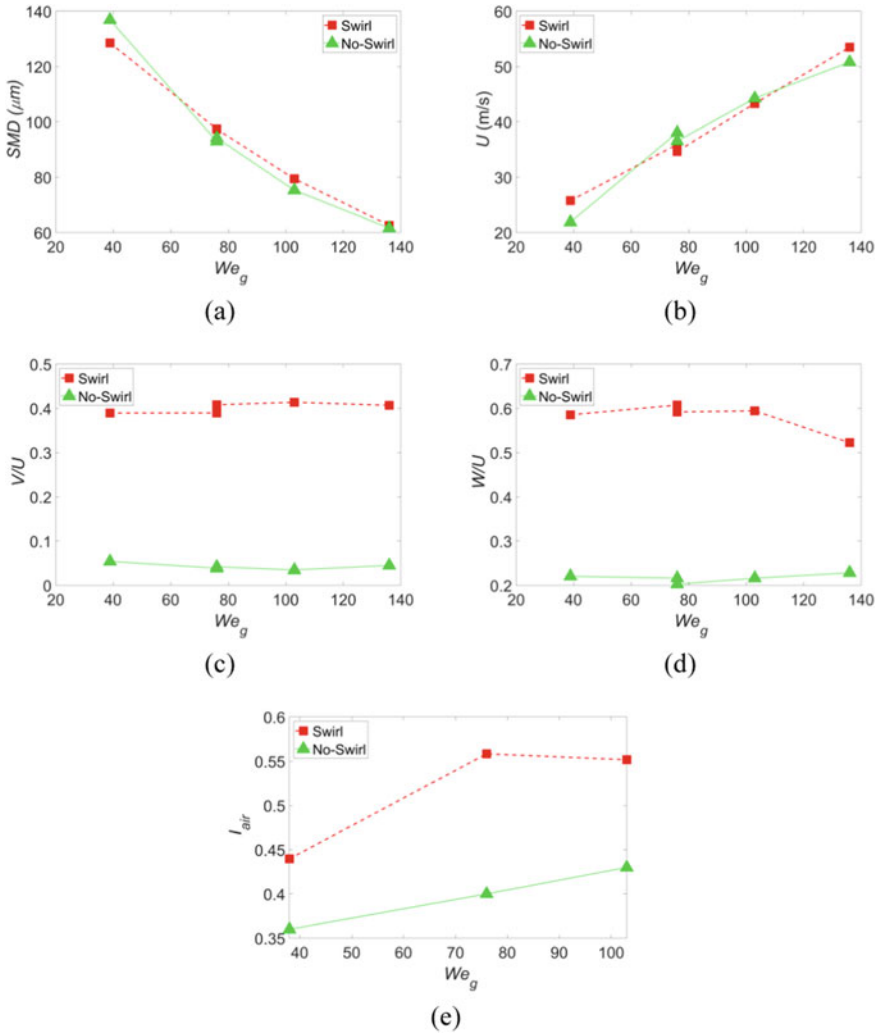
Fig. 2 Spray characterization at $X = 50$ mm, $R = 20$ mm **a** *SMD* versus We$_g$. **b** *U* versus We$_g$. **c** *V/U* versus We$_g$. **d** *W/U* versus We$_g$. **e** I_{air} versus We$_g$

W increases with We$_g$ and hence spray is expected to expand radially outwards and void is expected to form in central region of the atomizer. It is noted that as tangential and radial velocities in case of non-swirling crossflow are negligible, hence droplets are not expected to spread radially outwards, and instead droplets will be accumulated near the central region of the atomizer axis. Moreover, the turbulent intensity of air, I_{air} (based on axial velocity) is between 36 and 43% for non-swirling crossflow while for swirling crossflow I_{air} is between 44 and 55% when We$_g$ is varied from 38 to 103 at $X = 50$ mm and $R = 20$ mm as can be seen in Fig. 2e. I_{air} is almost 25%

higher for swirling crossflow as compared to non-swirling crossflow. I_{air} is the ratio between root mean square of axial velocity (U_{rms}) and mean axial velocity (U_{air}) of air. The statistical uncertainty in I_{air} is around 1%. Note that U_{rms} and U_{air} were measured using Laser Doppler Velocimetry (LDV) technique in which airflow alone (liquid flow rate into the atomizer was zero) was supplied into atomizer along with olive oil particles acting as tracers for airflow.

3.2 Application of POD Analysis

Figure 3 shows the mean spray image for swirling and non-swirling crossflows for Case 2 and Case 5. As discussed in Sect. 3.1, there is significant increase of tangential and radial velocity of droplets under the presence of swirling crossflow; hence, spray is dispersed radially outwards and void region is formed near the central region of atomizer as seen in Fig. 3a ($S = 0.74$). In case of non-swirling crossflow, due to
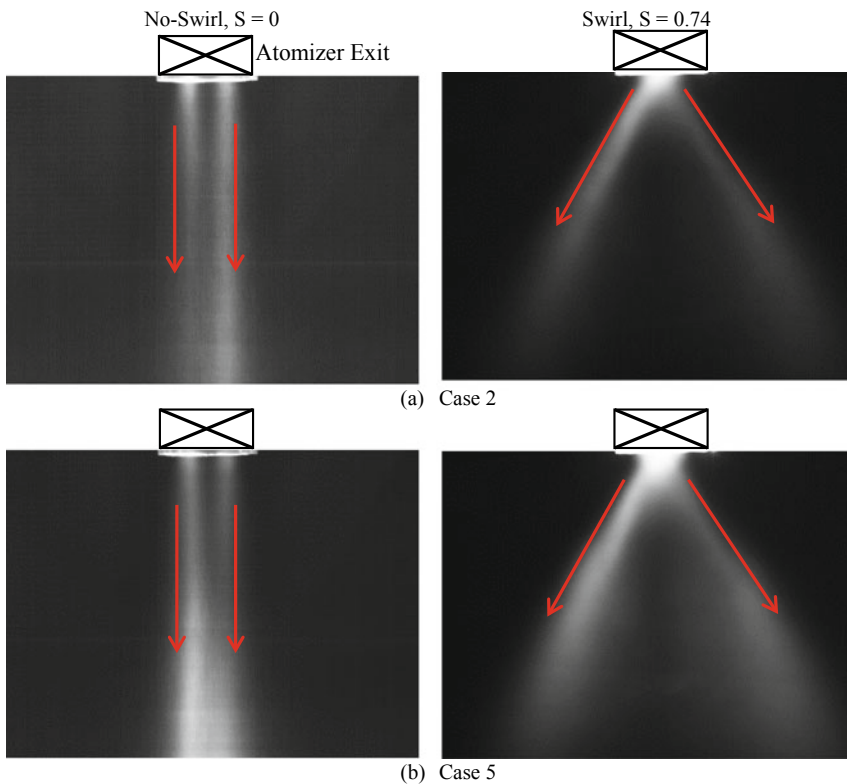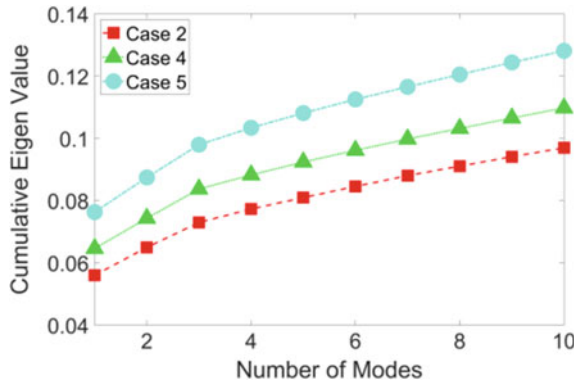

(a) Case 2

(b) Case 5

Fig. 3 Mean spray images for **a** Case 2 (We$_g$ = 76, MFR = 3.3). **b** Case 5 (We$_g$ = 136, MFR = 4.1)

Fig. 4 Cumulative eigen value versus number of modes for Case 2 (We$_g$ = 76, MFR = 3.3), Case 4 (We$_g$ = 103, MFR = 3.8) and Case 5 (We$_g$ = 136, MFR = 4.1)

the negligible tangential and radial velocity of droplets, spray is restricted to central region of atomizer as seen in Fig. 3a ($S = 0$). The droplet number density increases as indicated by the increase in intensity of mean image in Fig. 3b as the We$_g$ is increased from Case 2 (We$_g$ = 76) to Case 5 (We$_g$ = 136). The number of droplets increases and the void region in the central region of atomizer is no more visible in Fig. 3b ($S = 0.74$) possibly due to the formation of stronger recirculation zone in the central region of spray.

Figure 4 shows the variation of cumulative eigen value with the number of modes for Cases 2, 4, and 5. Eigen value represents the amount of energy present in that particular mode and in the context of spray images, energy means intensity of the pixels in an image. It can be observed that eigen value contribution for mode 1 increases as the We$_g$ is increased from Case 2 (We$_g$ = 76), Case 4 (We$_g$ = 103) to Case 5 (We$_g$ = 136). It implies that the pixel illumination or intensity of image which indicates the number density of image is increased as the We$_g$ is increased. It can be noticed that the cumulative eigen value contribution till ten modes is about 8, 10, and 13% for Case 2, Case 4, and Case 5, respectively. It means that as the We$_g$ is increased, higher energy is captured within few modes hence first few modes are sufficient to demonstrate the dominant features on spray while for lower We$_g$, more number of modes will be required to study dominant features of spray.

Figure 5 (First row) shows the contour plots of first four POD modes for Case 2. The first POD mode shows the mean structure of the spray as depicted by the mean image as shown in Fig. 3. The second and third POD modes show the breakup of ligaments and depict the region of concentrated droplet number density below the atomizer exit. The fourth POD mode shows the flapping of spray structure. The similar POD features of breakup and flapping of liquid jet were observed in context of liquid jet in crossflow [13]. It implies that the memory of breakup and flapping features is still retained in the spray structure downstream of the atomizer exit. The dominant structures and features shown by the first four POD modes can be understood by looking at the instantaneous spray images corresponding to the minimum negative coefficient ($\alpha_{min} < 0$) and maximum positive coefficient ($\alpha_{max} > 0$) of each POD mode as shown in Fig. 5 (second row) and Fig. 5 (third row),
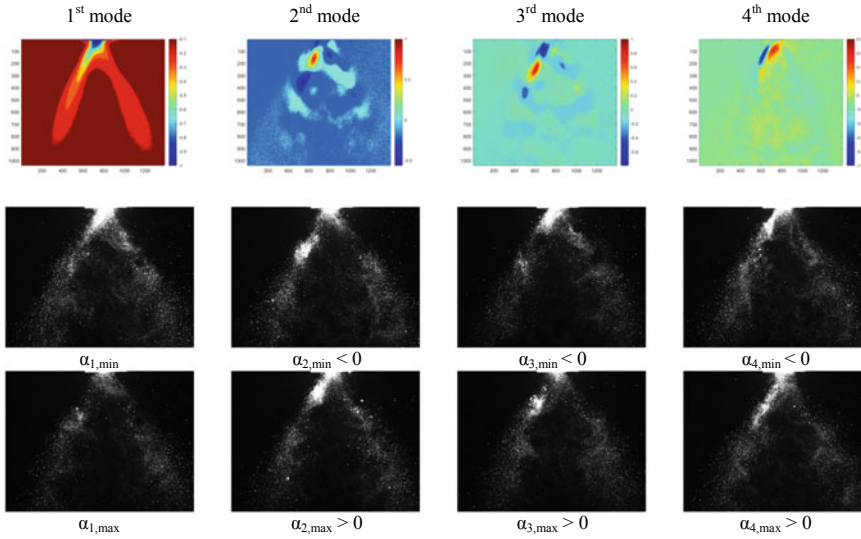
Fig. 5 First row: Contour plots for POD modes for Case 2 ($We_g = 76$, MFR = 3.3), Second row: Minimum negative coefficient for corresponding modes in first row, Third row: Maximum positive coefficients for corresponding modes in first row

respectively. It is noted for first mode that all the coefficients were negative. The droplet count is higher for $\alpha_{1,\min}$ while droplet count is observed less for $\alpha_{1,\max}$. It shows that first POD mode shows the fluctuations of droplet number at the exit of the atomizer. The second and third modes together represent shedding of ligaments further downstream of the exit of the atomizer. The region of concentrated droplet number density is away from the atomizer exit for $\alpha_{2,\min} < 0$ while the chunk of concentrated droplets is closer to atomizer exit for $\alpha_{2,\max} > 0$ (see Fig. 5). The vice versa is observed for third mode, i.e., the chunk of concentrated droplet is closer to atomizer exit for $\alpha_{3,\min} < 0$ while it is away from the atomizer exit for $\alpha_{3,\max} > 0$. Such features were observed for the liquid jet itself by Marco and Soteriou [14] in context of liquid jet breakup in crossflow where they reported that such alternate features depicted travelling waves on the liquid jet surface. It is clearly evident (from the alternate modal features of second and third mode) that the upstream liquid jet breakup process strongly affects the downstream spray characteristics. The spray structure can be seen to be tilted toward left side (near the atomizer exit) for $\alpha_{4,\min} < 0$, while the spray structure is tilted toward right side for $\alpha_{4,\max} > 0$ (see Fig. 5) which depicts the flapping behavior of spray structure.

Figure 6 (First row) shows first four POD modes for Case 5. Similar to Fig. 5 (Case 2), first POD mode shows the mean structure of the spray. Due to smaller size of droplets, the tangential and radial velocity are smaller (compared to Case 2), so centrifugal forces are negligible and hence such smaller sized droplets would be trapped in the central region of atomizer as the SMD reduces from Case 2 to Case 5 as shown earlier in Fig. 2 and hence more droplets are trapped near the central
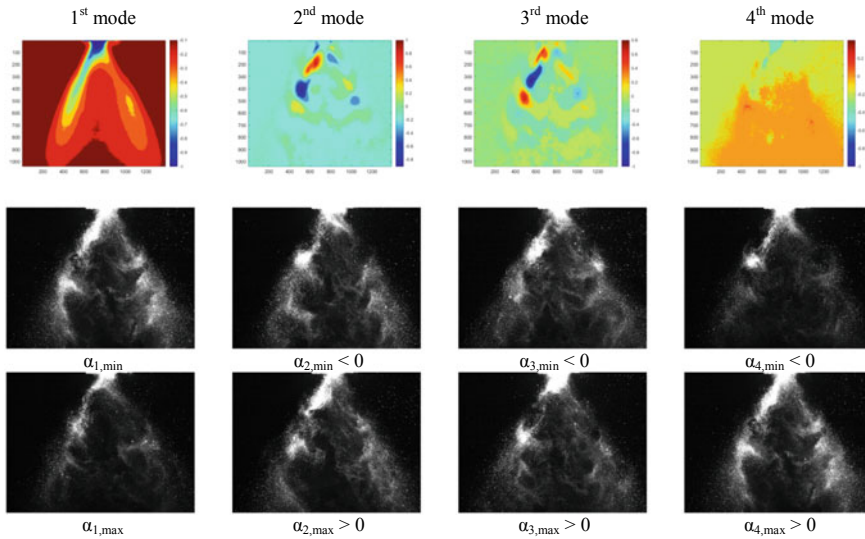
Fig. 6 First row: First four POD modes for Case 5 ($We_g = 136$, MFR = 4.1), Second row: Minimum negative coefficient for corresponding modes in first row, Third row: Maximum positive coefficients for corresponding modes in first row

region of atomizer. It is due to this reason that the void region was present in the central region of atomizer for Case 2 (see Fig. 5, first mode) while the central region of atomizer is filled with droplets for Case 5 (see Fig. 6, first mode). The fluctuations of droplet number is represented by $\alpha_{1,min}$ and $\alpha_{1,max}$ in Fig. 6 similar to Case 2 in Fig. 5. The alternate feature of the region with concentrated droplet number density is shown by second and third mode in Fig. 6 similar to Fig. 5. The fourth POD mode for Case 5 as shown in Fig. 6 showed the fluctuations in the droplet count while the flapping behavior of the spray structure is now shifted to fifth mode (not shown here). It means that for higher We_g, fluctuations in droplet count become dominant feature of the spray. The droplet count is observed less for $\alpha_{4,min} < 0$ while droplet count is significantly high and additionally, more droplet clusters can be seen for $\alpha_{4,max} > 0$. The fourth POD mode brings out very important feature of spray fluctuations which is otherwise cannot be captured by PDPA technique. Even though flow rates of water and air into the atomizer were maintained constant, significant difference in droplet number is observed from one instant to another which is due to different types of instabilities such as Kelvin-Helmholtz, Rayleigh-Taylor instabilities which govern the atomization process. These instabilities in spray may further cause spatially non-uniform mixing of fuel–air mixture which can lead to the formation of pockets with rich equivalence ratio and hence giving rise to the NO_x formation. The temporal variation in fuel–air mixing may lead to combustion instabilities inside gas turbine combustor [15]. In addition, due to the turbulent crossflow and interaction of turbulent eddies with droplets, preferential concentration of droplets may appear in some of the region in spray.

4   Conclusion

Optical measurements of spray characteristics are reported for a model twin-jet cross-stream airblast atomizer for LPP application. It was found that local *SMD* in the spray reduces for higher We$_g$ due to the change in breakup regimes of jet from bag breakup mode to surface breakup mode and further due to the secondary atomization. The *SMD* close to the injector exit was similar for swirling and non-swirling crossflows. The axial velocity of droplets increased with We$_g$ and it was similar for swirling and non-swirling crossflows. The tangential and radial velocity of droplets was significantly higher for swirling crossflow as compared to non-swirling crossflow and both velocities were found to increase with We$_g$. The spray structure indicated by second and third modes showed alternate region of concentrated droplet number density. The flapping of spray structure was observed in fourth mode. For higher We$_g$, spray, fluctuations are found to be more dominant.

References

1. Becker J, Hassa C (2002) Breakup and atomization of a kerosene jet in crossflow at elevated pressure. Atomization Sprays 12(1–3):49–68
2. Becker J, Heitz D, Hassa C (2004) Spray dispersion in a counter-swirling double-annular air flow at gas turbine conditions. Atomization Sprays 14(1):15–36
3. Elshamy OM, Tambe SB, Cai J, Jeng S-M (2007) PIV and LDV measurements for liquid jets in crossflow. In: 45th AIAA Aerospace Sciences Meeting and Exhibit, Reno, Nevada
4. Inamura T, Nagai N (1997) Spray characteristics of liquid jet traversing subsonic airstreams. J Propul Power 13(2):250–256
5. Tambe SB, Jeng S (2008) A study of liquid jets injected transversely into a swirling crossflow. In: 21st annual conference on liquid atomization and spray systems (April):1–12
6. Pei-Kuan W, Kirkendall KA, Fuller RP (1998) Spray structures of liquid jets atomized in subsonic crossflows. J Propul Power 14(2):173–182
7. Zheng Y, Marshall AW (2011) Characterization of the initial spray from low weber-number jets in crossflow 21(7):575–589
8. Batarseh FZ, Gnirß M, Roisman IV, Tropea C (2009) Fluctuations of a spray generated by an airblast atomizer. Exp Fluids 46(6):1081–1091
9. Patil S, Sahu S (2019) Breakup dynamics and near nozzle spray fluctuations in a twin-jet crossflow airblast atomizer. Atomization Sprays 29(3):217–250
10. Mazallon J, Dai Z, Faeth GM (1999) Primary breakup of nonturbulent round liquid jets in gas crossflows. Atomization Sprays 9:291–311
11. Sallam KA, Aalburg C, Faeth GM (2004) Breakup of round nonturbulent liquid jets in gaseous crossflow. AIAA J 42(12):2529–2540
12. Wu P-K, Kirkendall KA, Fuller RP, Nejad AS (1997) Breakup processes of liquid jets in subsonic crossflows. J Propul Power 13(1):64–73
13. Patil S, Sahu S (2018) Breakup dynamics in a twin-jet crossflow airblast atomizer. ICLASS 2018. In: 14th triennial international conference on liquid atomization and spray systems, Chicago, IL, USA
14. Arienti M, Soteriou MC (2009) Time-resolved proper orthogonal decomposition of liquid jet dynamics. Phys Fluids 21(11):1–15
15. Huang Y, Yang V (2009) Dynamics and stability of lean-premixed swirl-stabilized combustion. Prog Energy Combust Sci 35(4):293–364